

# Preliminary Search for $\tilde{\chi}_1^0 \rightarrow \tilde{\tau}\tau$ in Light Gravitino Scenarios

**Gustavo Wolf**

C.E.R.N.

## **Abstract**

Lightest neutralino pair production is searched for within the light gravitino scenario. It is assumed that the lightest neutralino is the NNLSP and that the  $\tilde{\tau}_1$  is the NLSP. Data at 183 GeV centre of mass energy are analysed and two candidates are found. Limits on the lightest neutralino pair production cross section are set at 95% CL, as a function of  $m_{\tilde{\chi}_1^0}$  and  $m_{\tilde{\tau}_1}$ .

# 1 Introduction

If supersymmetry at the electro-weak scale is established, one of the most important questions to address experimentally is the scale and mechanism of supersymmetry breaking. It is often assumed that the messengers of supersymmetry breaking interact with gravitational strength and that the breaking scale in a hidden sector is of the order of  $10^{11}$  GeV/ $c^2$ . An alternative possibility is that supersymmetry is broken at some low scale (between the Plank and the electro-weak scale), and that the ordinary gauge interaction acts as the messenger of supersymmetry breaking [1, 2]. In local supersymmetry, the Goldstino ( $\tilde{G}$ ) becomes the longitudinal component of the gravitino. In this case, the gravitino is naturally the lightest supersymmetric particle (LSP) and the lightest standard model superpartner is the next to lightest supersymmetry particle (NLSP). Then, the NLSP is unstable and decays to its SM partner plus a Goldstino.

Since the Goldstino couplings are suppressed compared to electro-weak and strong interactions, decays to the Goldstino are only relevant for the NLSP and therefore the production of pairs of supersymmetric particles at high energy colliders would generally take place through standard model couplings<sup>1</sup>. The supersymmetric particles cascade to NLSP's, that eventually decay to their SM partners and a Goldstino. The specific signatures of such decays depend crucially on the quantum numbers and composition of the NLSP, which are model dependent. This opens up the possibility to detect  $\tilde{\chi}_1^0\tilde{\chi}_1^0$  pair-production from its decay products, unlike in SUGRA models.

Although most of the attention has been focused on the case where the neutralino is the NLSP, it is equally possible that the NLSP is any other sparticle, and in particular a charged lepton. The number of  $5 + \bar{5}$  generations of gauge mediating messengers, over most of the parameter space, determines what particle is the NLSP [4, 5, 6, ?]. For example, for one generation of  $5 + \bar{5}$  the lightest neutralino tends to be the NLSP, while for two or more generations the balance tips towards right handed sleptons.

Throughout this work, it will be assumed that the  $\tilde{\tau}_1$  is the NLSP, and that the lightest neutralino ( $\tilde{\chi}_1^0$ ) is the *next-to*-NLSP (NNLSP).

This note describes the search for  $\tilde{\chi}_1^0$ -pair production, followed by the decay  $\tilde{\chi}_1^0 \rightarrow \tilde{\tau}\tau$ . The  $\tilde{\tau}$  decays promptly into  $\tilde{\tau} \rightarrow \tau\tilde{G}$ . Long lived decays of the  $\tilde{\tau}$  will be studied in a future work. The search for direct pair production of  $\tilde{\tau}$ 's is described elsewhere [7]. The former search is complementary to the later in regions where  $\tilde{\tau}$ - pair production has small cross section.

Thus, the signature of the signal is four  $\tau$ 's plus missing energy and momentum from the two gravitinos (plus the energy and momentum carried away by the neutrinos of the decay of the  $\tau$ 's).

The experimental procedure and event selection are described in section 2 and the results are presented in section 3.

## 2 Experimental procedure and event sample

The analysis is based on data collected by DELPHI during 1997 at a centre of mass energies 183 GeV/ $c^2$ . The total integrated luminosity for this period is 53.9  $pb^{-1}$ . A

---

<sup>1</sup>One exception to this rule being the process  $e^+e^- \rightarrow Z^0/\gamma^* \rightarrow \tilde{G}\tilde{\chi}_1^0$ , for the case of ultra-light  $\tilde{G}$ , which will be studied in a future work.

detailed description of the DELPHI detector can be found in [8] and its performance in [9].

To evaluate the signal efficiencies and background contaminations, events were generated using several different programs. All relied on JETSET 7.4 [10], tuned to LEP 1 data [11], for quark fragmentation. The program SUSYGEN [12] was used to generate the neutralino-pair events, and their subsequent decay products. In order to compute detection efficiencies, a total of 14,000 events with centre of mass energy  $184 \text{ GeV}/c^2$  and masses  $45 \text{ GeV}/c^2 \leq m_{\tilde{\tau}} \leq m_{\tilde{\chi}_1^0} - 2 \text{ GeV}/c^2$ ,  $m_{\tilde{\tau}} + 2 \text{ GeV}/c^2 \leq m_{\tilde{\chi}_1^0} < \text{sqrts}/2$ .

The background process  $e^+e^- \rightarrow q\bar{q}(n\gamma)$  was generated with PYTHIA 5.7 [10], while DYMU3[14] and KORALZ[15] were used for  $\mu^+\mu^-(\gamma)$  and  $\tau^+\tau^-(\gamma)$ , respectively. The generator of Ref. [16] was used for  $e^+e^- \rightarrow e^+e^-$  events.

Processes leading to four-fermion final states,  $(Z/\gamma)^*(Z/\gamma)^*$ ,  $W^+W^-$ ,  $W\nu_e$  and  $Ze^+e^-$ , were also generated using PYTHIA. The calculation of the four-fermion background was verified using the program EXCALIBUR [17], which consistently takes into account all amplitudes leading to a given four-fermion final state.

Two-photon interactions leading to hadronic final states were generated using TWOGAM [18], separating the VDM, QPM, and QCD components. The generators of Berends, Daverveldt and Kleiss [19] were used for the leptonic final states.

The generated signal and background events were passed through the detailed simulation [13] of the DELPHI detector [8] and then processed with the same reconstruction and analysis programs as the real data.

## 2.1 Data selection

The following cuts were applied in order to reduce the SM background preserving the signal efficiency:

As a Preselection: To assure good quality of the data, the ratio of good charged tracks [20] to total number of tracks was required to be above 0.7 <sup>2</sup>. The events were also to have at least 4 and at most 10 good charged tracks. In addition, in order not to process the bulk of the events of both data and background MCs, the thrust, the transverse momentum and the absolute value of the cosine of the  $\theta$  angle of the missing momentum vector ( $\theta_{miss}$ ) were required to respectively be smaller than 0.9, bigger than 3 GeV/c, and smaller than 0.95. Very forward-going events were eliminated by requiring that the energy in a cone of  $30^\circ$  around the beam-pipe be less than 70% of the total visible energy. With this preselection, around 1 event in 6,000 were recorded and analysed.

In order to optimise the cuts, it was noticed that signal events can be separated into two different kinematic regions of the  $m_{\tilde{\chi}_1^0}$  vs.  $m_{\tilde{\tau}_1}$  space: when the mass difference  $\Delta_m = m_{\tilde{\tau}_1} - m_{\tilde{\chi}_1^0}$  is around or bigger than 10 GeV, all 4  $\tau$ 's carry similar momenta. When the difference becomes smaller, the two  $\tau$ 's coming from the decay of the  $\tilde{\tau}_1$  tend to be the most energetic, the more with increasing  $\tilde{\chi}_1^0$  mass. We used the Durham algorithm to divide the event in four jets. Numbering the jets from 1 to 4 with  $E_1 > \dots > E_4$ , we

---

<sup>2</sup>In DAFNE, charged tracks that do not pass quality cut selection but have an associated calorimetric energy of at least 2 GeV are recovered and their momentum is recalculated as this associated energy. Our definition of a good track does not include recovered tracks, but they are used in the calculation of all kinematic variables.

defined the following variable  $r$ :

$$r = \frac{E_3 + E_4}{E_1 + E_2} \quad (1)$$

An example of the distribution of  $r$  for two  $\Delta_m$  can be seen in Fig. 1. The background MC samples were then divided into two samples above and below  $r = 0.1$  and cuts on a given variable were set to different values when necessary.

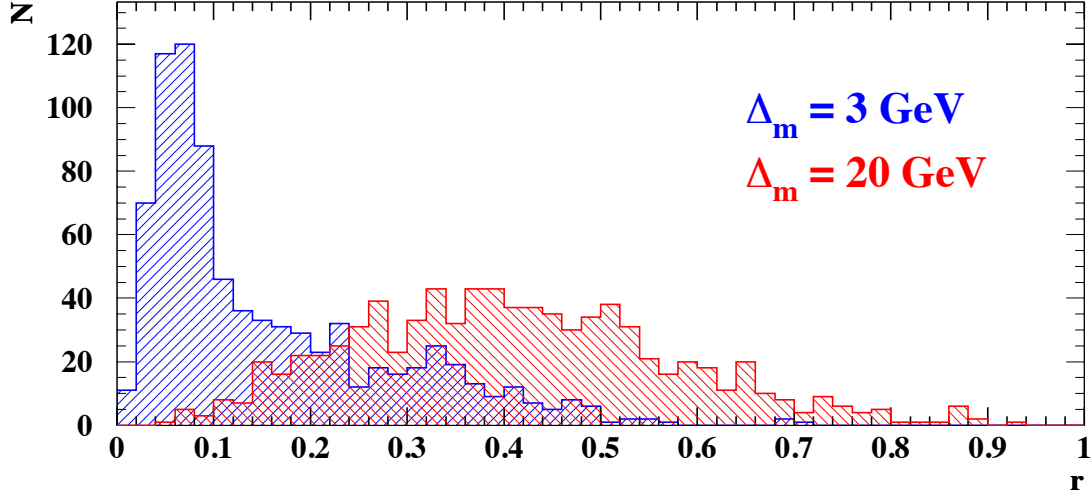


Figure 1: Distribution of the variable  $r$  for two values of  $\Delta_m$ .

Two sets of cuts were applied in order to reduce the  $\gamma\gamma$  and  $f\bar{f}(\gamma)$  backgrounds and a third set of cuts to select events according to their topology:

1. Cuts against  $\gamma\gamma$  backgrounds: The transverse energy ( $E_T$ ) should be bigger than 11 GeV for  $r > .1$  ( $E_T > 12$  GeV for  $r \leq .1$ ). The energy in a cone of  $30^\circ$  around the beam-pipe was further restricted to be less than 60% of the total visible energy to avoid possible bias from the MC samples. The missing mass should be smaller than  $0.88\sqrt{s}$  ( $0.9\sqrt{s}$ ). The momentum of the largest momentum track should be bigger than 4 GeV/c (3 GeV/c). After these cuts, the  $\gamma\gamma$  background is reduced by a factor of the order of 30.
2. Cuts against  $f\bar{f}(\gamma)$  backgrounds: The number of good charged tracks should be smaller than 7 (9). The thrust was further reduced from 0.99 to 0.975. At the 2-jet level, the acoplanarity should be bigger than  $8^\circ$ . The missing mass of the events should be bigger than  $0.3\sqrt{s}$ . After these cuts, the  $f\bar{f}(\gamma)$  background was reduced by a factor of the order of 15.
3. Cuts based on topology: Signal events tend naturally to cluster into a 4-jet topology. We asked all jets to be at least  $17^\circ$  away from the beam-pipe direction. We also asked that when reduced by a jet algorithm into a 2-jet configuration, each of these

jets should be broader than  $20^\circ$ . Finally, we asked each jet to be separated from the others at least by  $8^\circ$  ( $4^\circ$ ).

Figs. 2 to 6 show the distributions corresponding to these selection cuts. Table 1 shows the evolution of the data, expected background and one of the signal samples throughout these cuts.

Cut	$\gamma\gamma$	$ff\gamma$	4-fermion	Total MC	Data	Signal
pre-selection	$496 \pm 16$	$44.5 \pm 1.5$	$13.1 \pm 0.6$	$554 \pm 16$	567	61.4%
1	$18 \pm 2$	$40.6 \pm 1.4$	$12.1 \pm 0.6$	$70.8 \pm 2.6$	84	59.2%
2	$2.2 \pm 0.6$	$2.9 \pm 0.4$	$4.5 \pm 0.4$	$9.6 \pm 0.8$	12	45.4%
3	0	$0.23 \pm 0.09$	$0.27 \pm 0.07$	$0.50 \pm 0.11$	2	38.3%

Table 1: Evolution of data and MC through the different cuts described in the text. Signal corresponds to  $m_{\tilde{\chi}_1^0} = 75\text{GeV}/c^2$  and  $m_{\tilde{\tau}} = 55\text{GeV}/c^2$ .

After these cuts, an efficiency between 25 and 45% was obtained for the signal events, and an estimated background of  $.50 \pm 0.11$ .

### 3 Results

Two data events were observed to pass all the cuts. They are shown in figs. 7 to 10. Their main features are listed in Table 2. They can be interpreted as being 4-fermion events. The first one, has an electron, a low energy particle that could either be a muon or a pion, a pion and a very soft particle that cannot be identified. It could be described as a  $\gamma^*\gamma^*$  event, each one going into a pair of  $\tau$ s. The second event, has one muon, two energetic electrons and a pion. It could be described as a  $Z\gamma^*$  event, with  $Z \rightarrow e^+e^-$ , and  $\gamma^* \rightarrow \tau^+\tau^-$ .

Since no evidence for a signal was found in the data, a limit on the production cross section for neutralino pairs was derived for each  $m_{\tilde{\chi}_1^0}, m_{\tilde{\tau}_1}$  combination. A statistical error of 1.5% was assumed for the signal efficiency. Twice this amount was subtracted in order to derive the limits.

Fig. 11 shows the limit at the 95% CL on  $\tilde{\chi}_1^0$ -pair production cross section, as a function of  $m_{\tilde{\chi}_1^0}$  and  $m_{\tilde{\tau}}$  at  $\sqrt{s} = 183$  GeV.

Limits can also be obtained within certain models. As an example, fig. 12 shows the 95% C.L. excluded areas for the case n=2 in the  $m_{\tilde{\chi}_1^0}$  vs.  $m_{\tilde{\tau}_1}$  plane. The purple area is excluded by this analysis. Only gaugino-like neutralinos are taken into account. The dashed-purple line shows the predicted limit. For higgsino-like neutralinos, there is no limit above 45 GeV. The red area is excluded by the analysis searching for neutralino-pair production followed by the decay  $\tilde{\chi}_1^0 \rightarrow \tilde{G}\gamma$  [22]. The dashed-red line shows where the exclusion would be in the case of higgsino-like neutralinos. The blue area is excluded by the direct search for  $\tilde{\tau}_1$ -pair production [23]. Conventions follow the ones of a GMSB model described in [5]. n is the number of messenger generations. The lower limit for the lightest neutralino is at 76 GeV for n=2. In the case of higgsino-like neutralinos, the blue region extends up to the diagonal and the limit becomes 67 GeV.

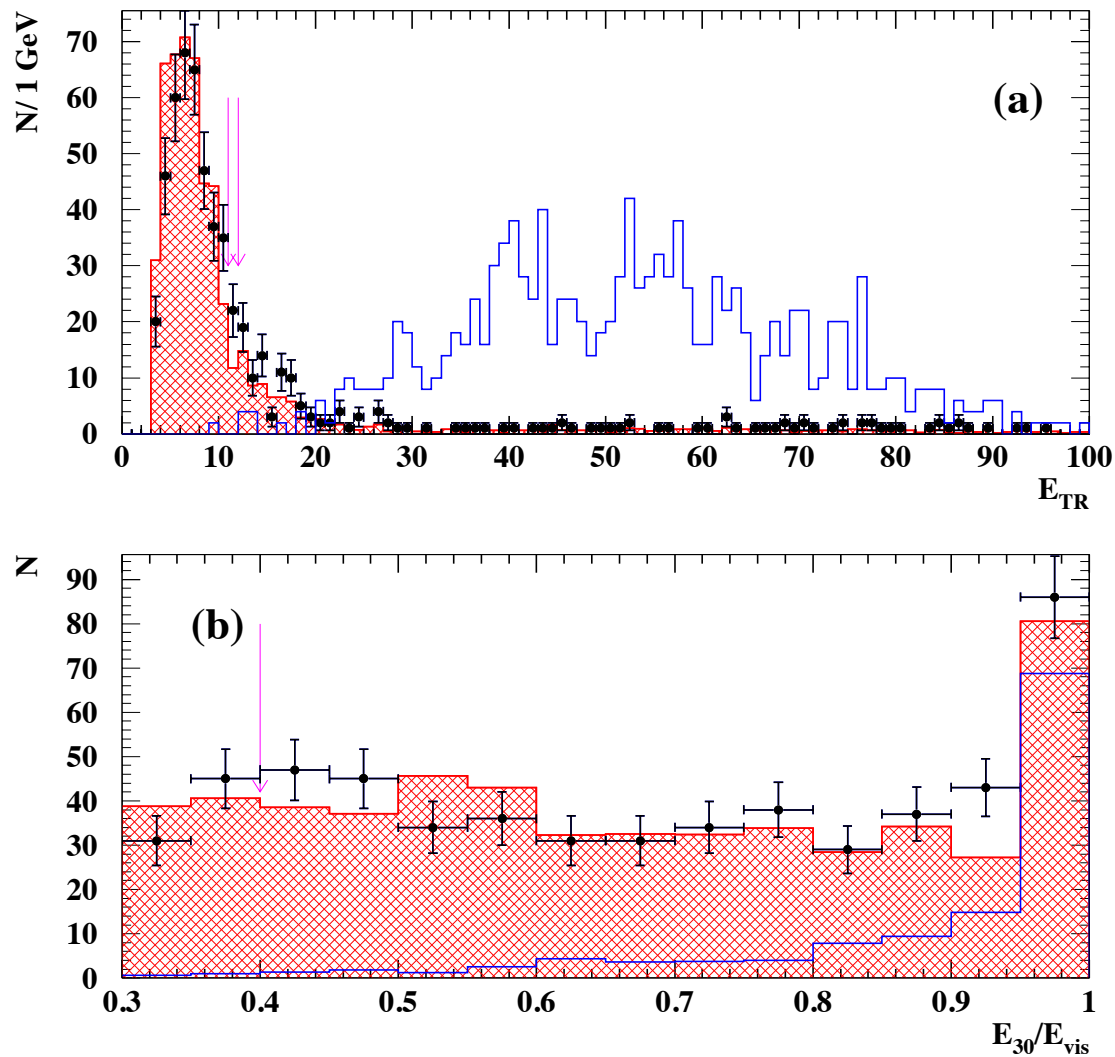


Figure 2: Transverse Energy (a) and Energy outside a cone of  $30^\circ$  over the total visible energy (b) for data (dots), SM MC (red shaded) and one of the simulated signals with cross section not to scale (blue) after preselection. Cuts for these variables are explained in the text and are shown with purple arrows.

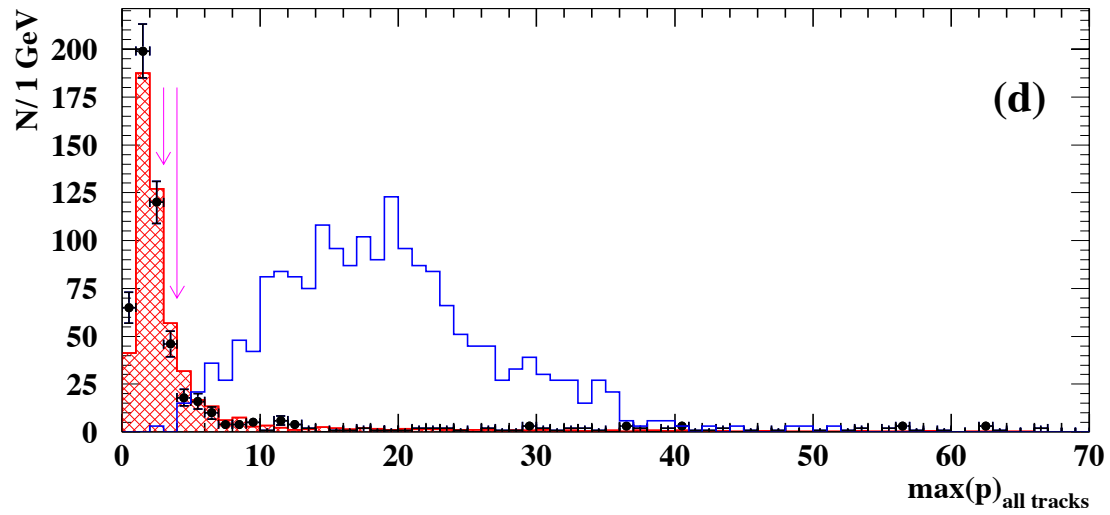
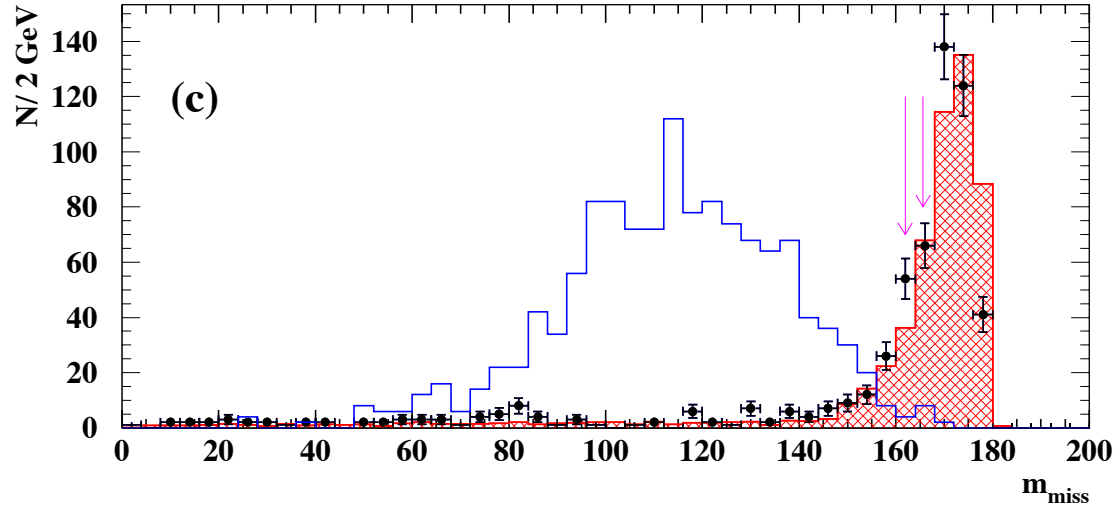


Figure 3: Missing Mass (c) and Momentum of the charged track with largest momentum (d) for data (dots), SM MC (red shaded) and one of the simulated signals with cross section not to scale (blue) after preselection. Cuts for these variables are explained in the text and are shown with purple arrows.

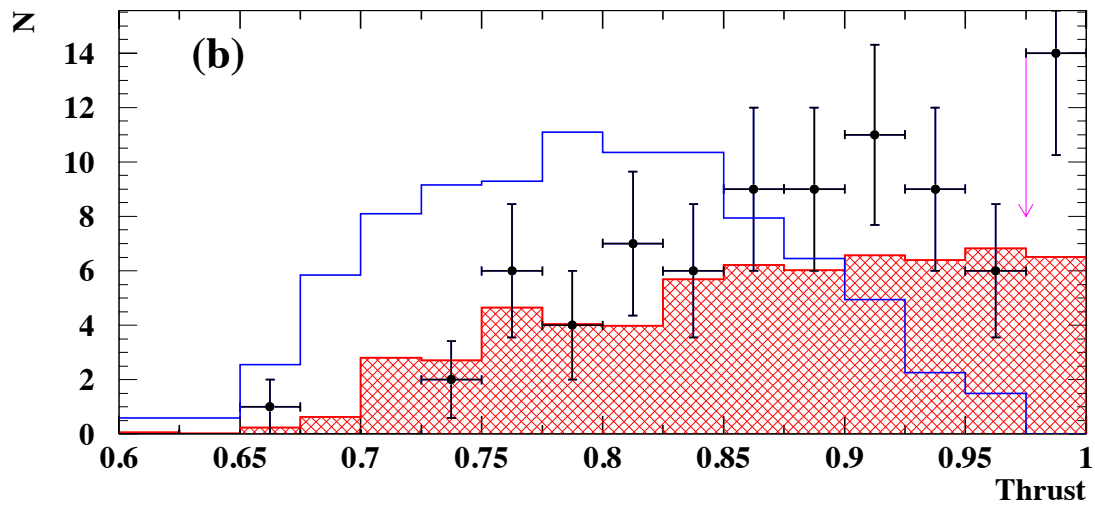
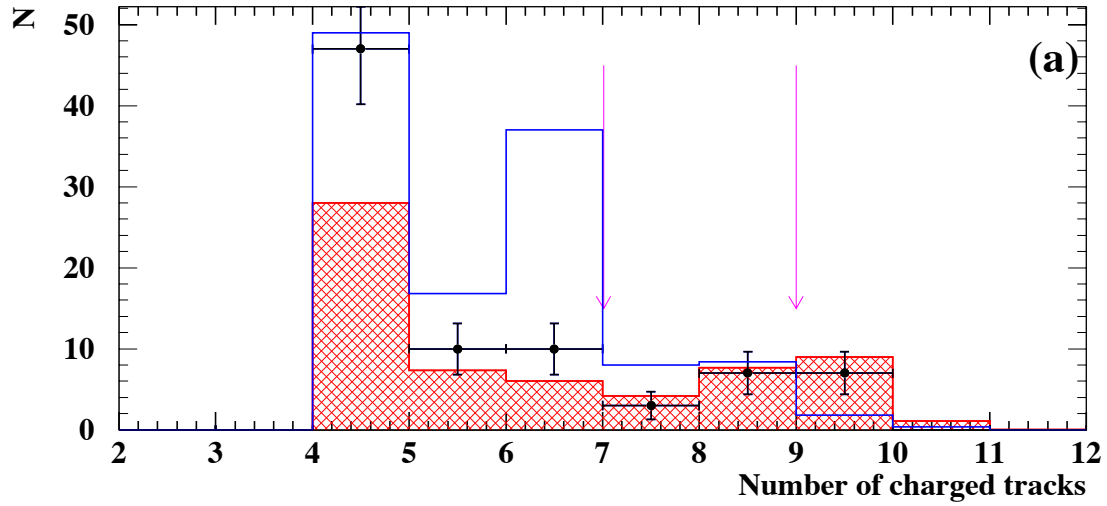


Figure 4: Number of charged tracks (a) and Thrust (b) for data (dots), SM MC (red shaded) and one of the simulated signals with cross section not to scale (blue), after the cut to remove  $\gamma\gamma$  events. Cuts for these variables are explained in the text and are shown with purple arrows.



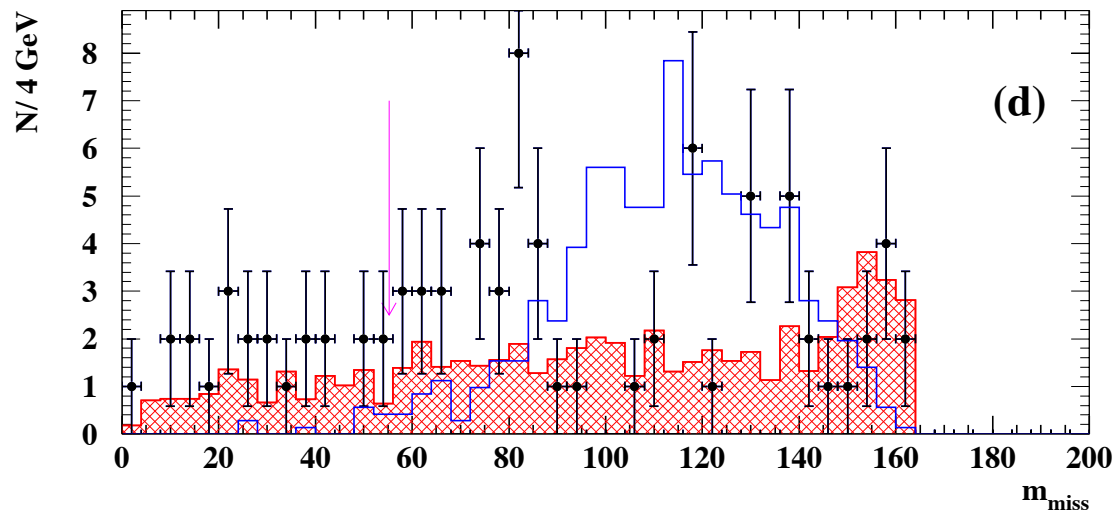
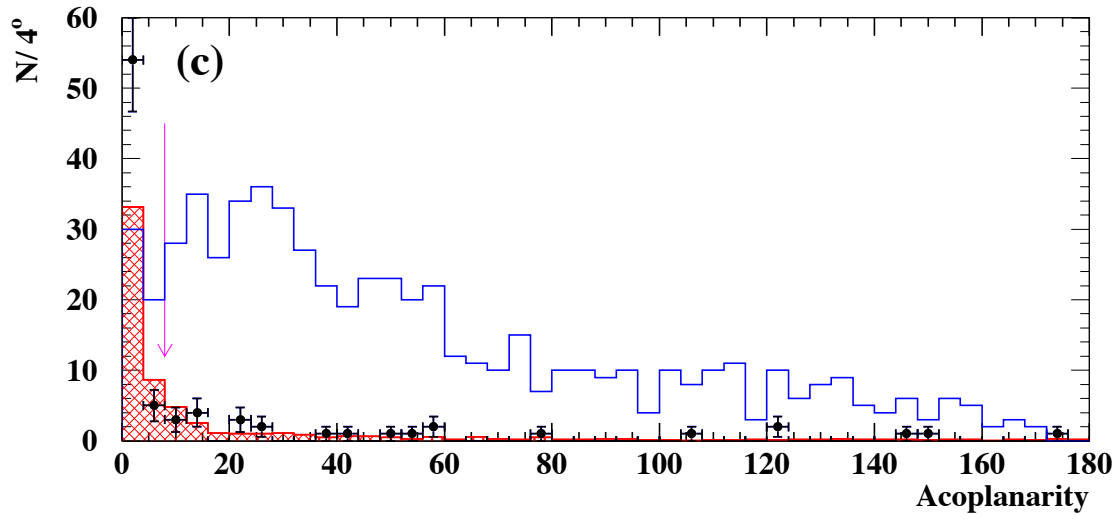


Figure 5: Acoplanarity (c) and Missing Mass (d) for data (dots), SM MC (red shaded) and one of the simulated signals with cross section not to scale (blue), after the cut to remove  $\gamma\gamma$  events. Cuts for these variables are explained in the text and are shown with purple arrows.

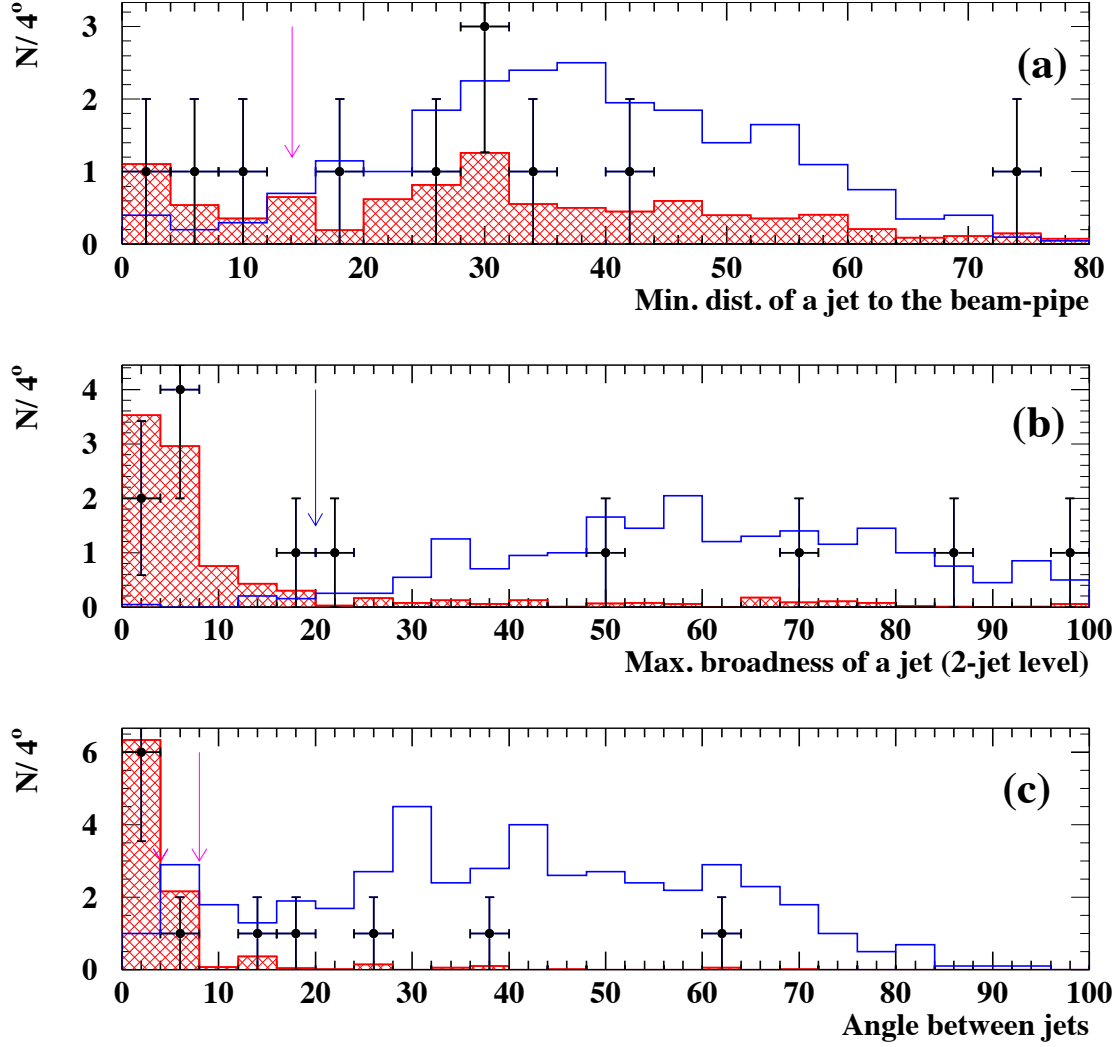



Figure 6: Minimum angular distance of a jet to the beam-pipe (a), Maximum angular broadness of a jet at the 2-jet level (b) and Angle between jets (c) for data (dots), SM MC (red shaded) and one of the simulated signals with cross section not to scale (blue), after the cut to remove  $f\bar{f}(\gamma)$  events. Cuts for these variables are explained in the text and are shown with purple arrows.

	<b>DELPHI</b>	<b>Run: 77798</b>	<b>Evt: 3574</b>							
	Beam: 91.6 GeV	Proc: 19-Jan-1998								
	DAS: 14-Sep-1997	Scan: 1-Feb-1998								
	18:45:01	Tan+DST								

	TD	TE	TS	TK	TV	ST	PA
Act	0	21	0	10	0	0	0
	( 84 )	(107 X	0 )	( 13 X	0 X	0 X	0 )
Deact	0	0	0	0	0	0	0
	( 0 X	0 X	0 X	0 X	0 X	0 X	0 )

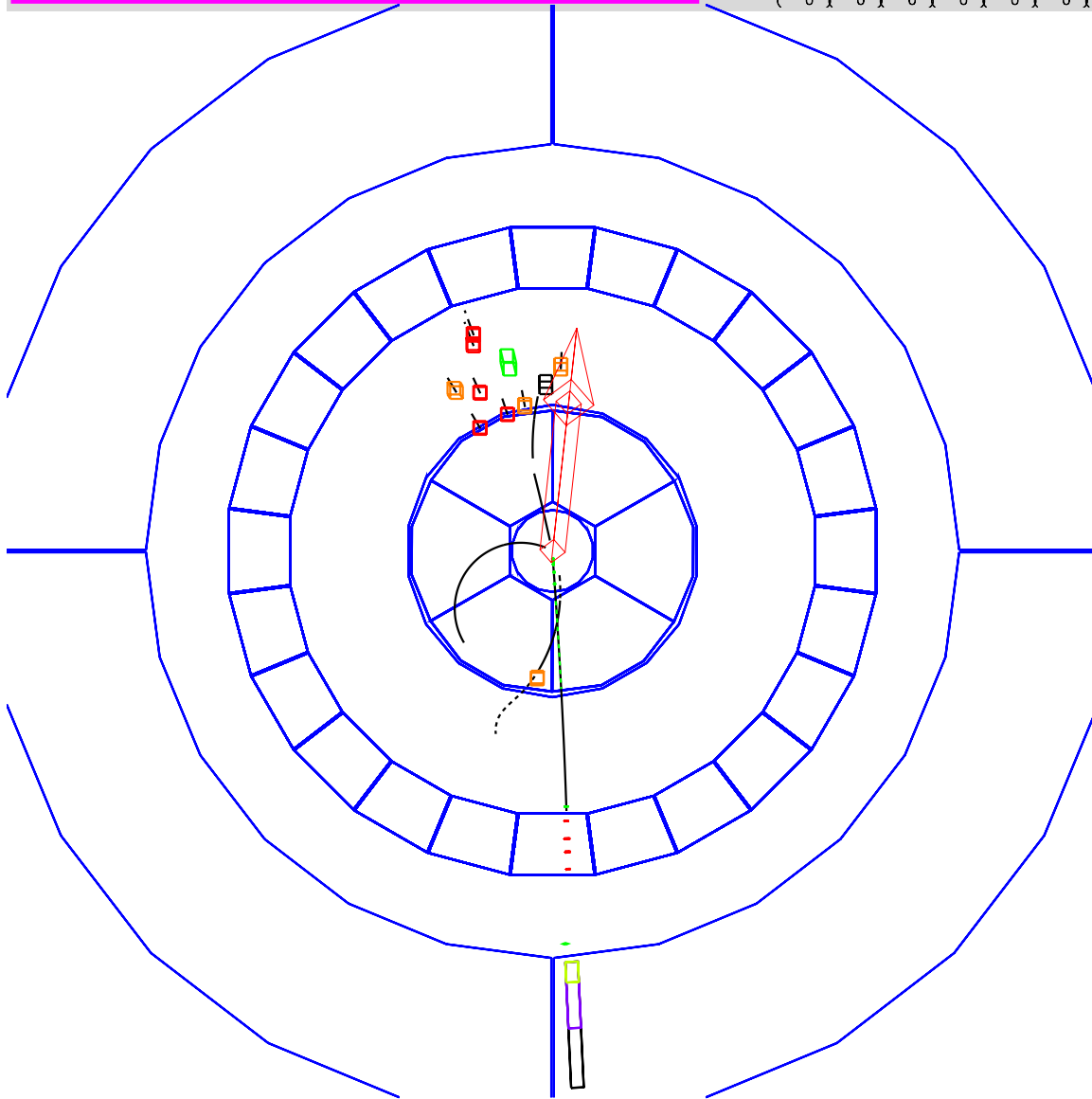



Figure 7: xy view of the first of the two candidates.

 <b>DELPHI</b>	<b>Run :</b> 77798	<b>Evt :</b> 3574							
	<b>Beam:</b> 91.6 GeV	<b>Proc:</b> 19-Jan-1998							
	<b>DAS:</b> 14-Sep-1997	<b>Scan:</b> 1-Feb-1998							
	<b>18:45:01</b>	<b>Tan+DST</b>							

	TD	TE	TS	TK	TV	ST	PA
Act	0	93	0	10	0	0	0
	( 84 )	(107 X	0 )	( 13 X	0 X	0 X	0 )
Deact	0	0	0	0	0	0	0
	( 0 X	0 X	0 X	0 X	0 X	0 X	0 )

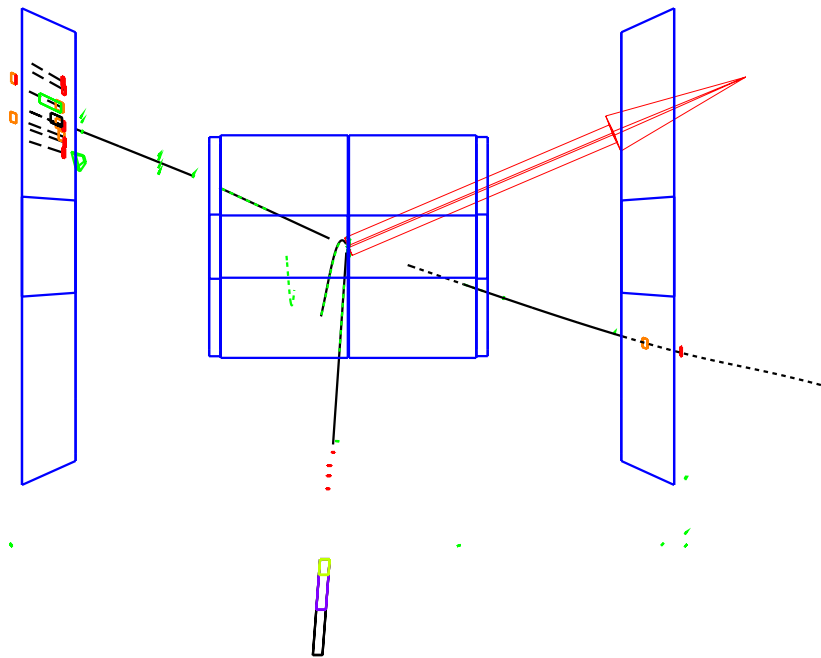



Figure 8: yz view of the first of the two candidates.

	<b>DELPHI</b>	<b>Run: 78409</b>	<b>Evt: 10676</b>								
	Beam: 91.6 GeV	Proc: 20-Jan-1998									
	DAS: 26-Sep-1997	Scan: 1-Feb-1998									
	03:24:40	Tan+DST									

	TD	TE	TS	TK	TV	ST	PA
Act	0	96	0	6	0	0	0
	( 93 )	(109 Y	0 Y	6 Y	0 Y	0 Y	8 )
Deact	0	0	0	0	0	0	0
	( 0 Y	0 Y	0 Y	2 Y	0 Y	0 Y	0 )

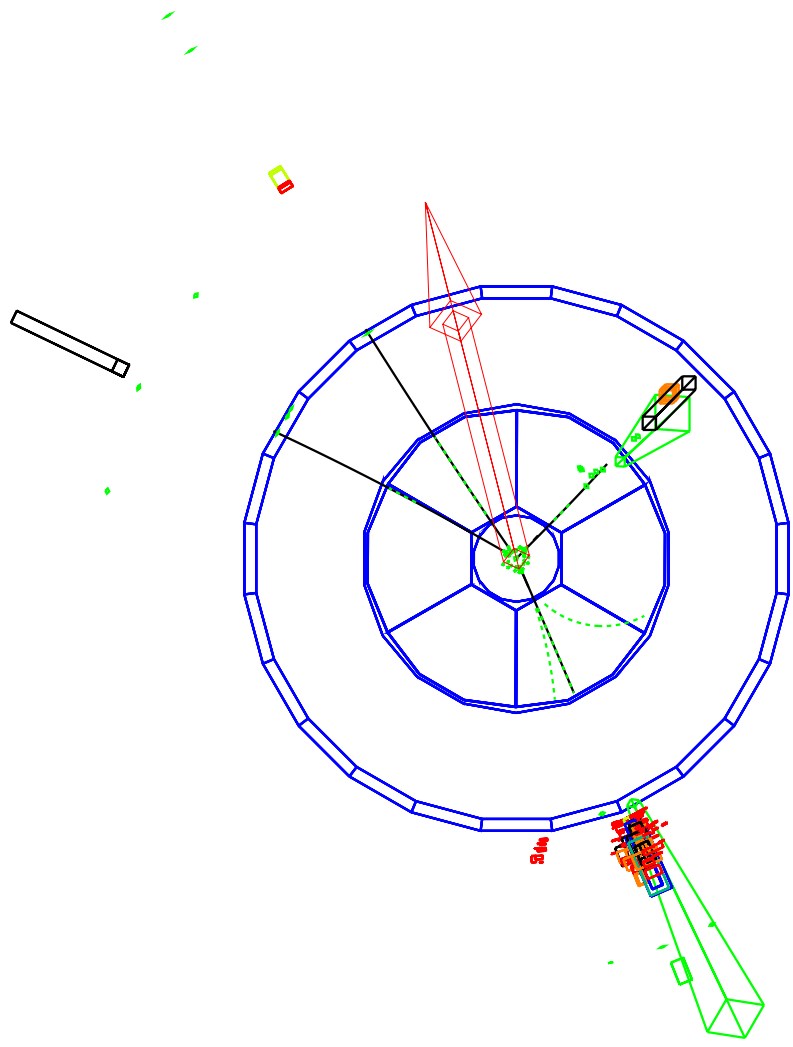



Figure 9: xy view of the second of the two candidates.

	<b>DELPHI</b>	<b>Run: 78409</b>	<b>Evt: 10676</b>								
	Beam: 91.6 GeV	Proc: 20-Jan-1998									
	DAS: 26-Sep-1997	Scan: 1-Feb-1998									
	03:24:40	Tan+DST									

	TD	TE	TS	TK	TV	ST	PA
Act	0	96	0	6	0	0	0
	( 0 )	(109 Y	0 Y	6 Y	0 Y	0 Y	8 )
Deact	0	0	0	0	0	0	0
	( 0 Y	0 Y	0 Y	2 Y	0 Y	0 Y	0 )

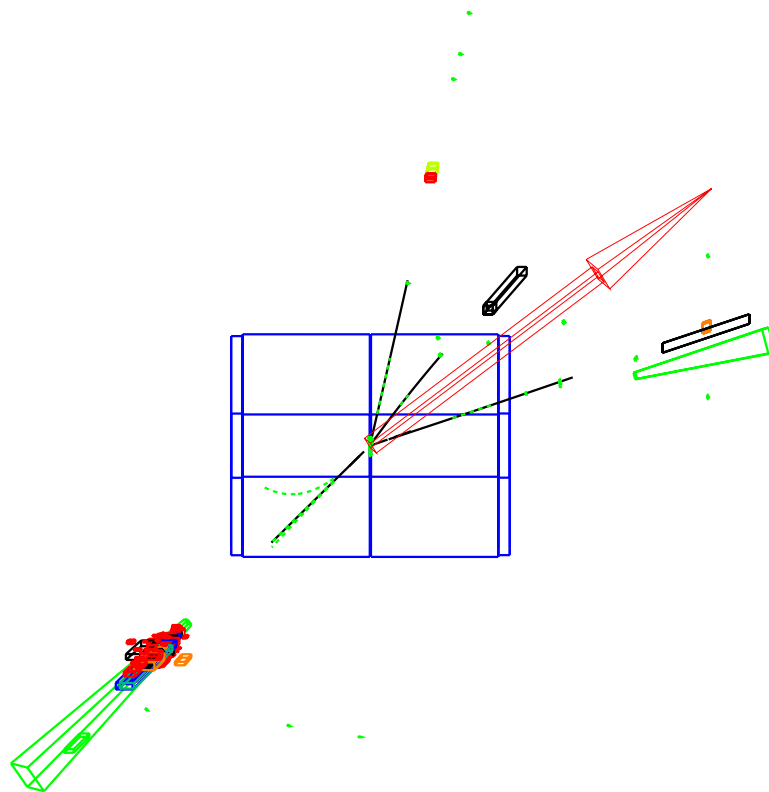


Figure 10: xz view of the second of the two candidates.

	Candidate 1	Candidate 2
$r$	.14	.31
$p_T$	8.7	9.2
$m_{miss}$	139.5	63.8
thrust	0.91	0.84
$E_{30}/E_{vis}$	0.45	0.62
$E_{TR}$	28.	78.6
acoplanarity	$8.6^\circ$	$15.9^\circ$
Num. of charged tracks	4	6
Min. angle between jets	$63^\circ$	$26.^\circ$
P of track with max momentum	17.8	43.7

Table 2: Some characteristics of the two candidates.

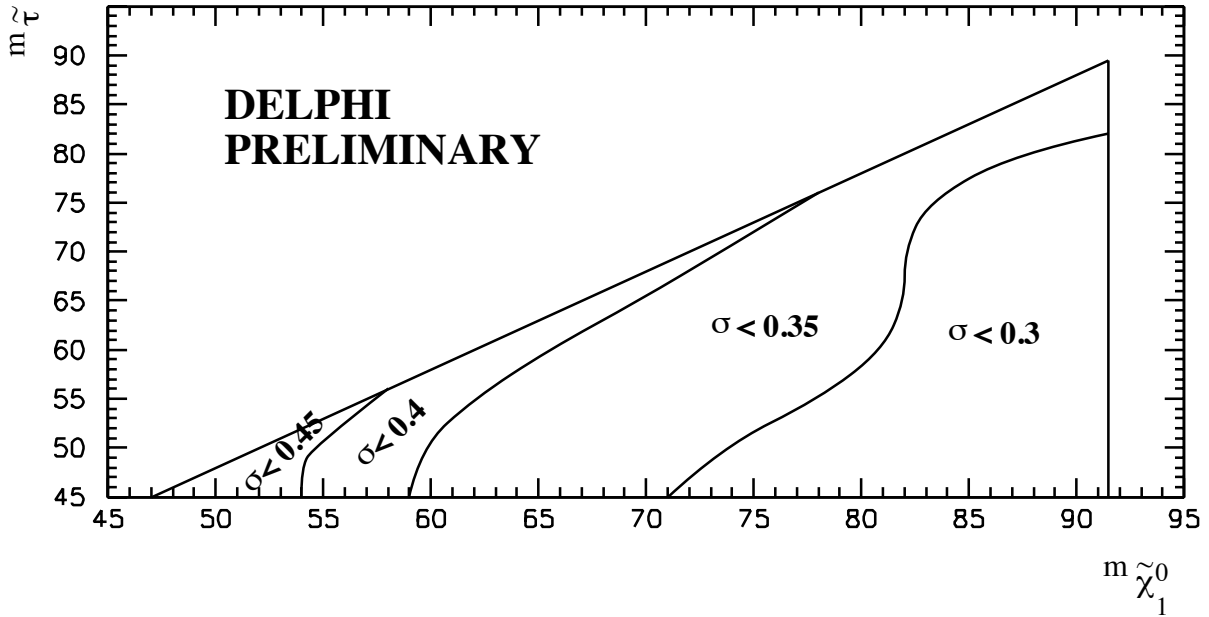


Figure 11: Limit at the 95% CL on  $\tilde{\chi}_1^0$ -pair production cross section at  $\sqrt{s} = 183$  GeV, as a function of  $m_{\tilde{\chi}_1^0}$  and  $m_{\tilde{\tau}_1}$ .

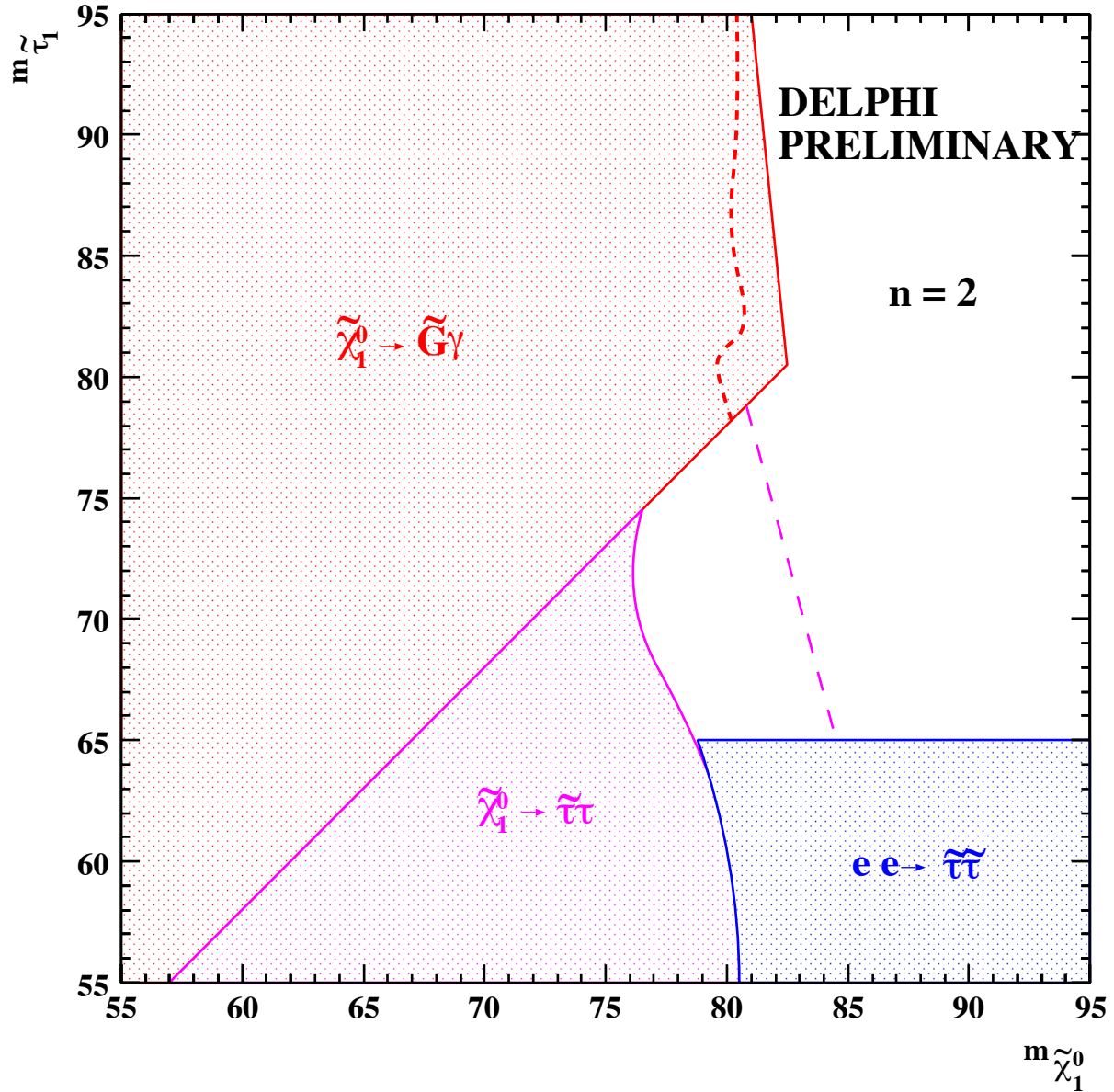


Figure 12: Areas excluded at the 95% CL for  $n=2$  in the  $m_{\tilde{\chi}_1^0}$  vs.  $m_{\tilde{\tau}_1}$  plane. The purple area is excluded by this analysis for gaugino-like neutralinos. The purple dashed line is the expected limit. The red area is excluded by the search for acoplanar photons (the red dashed line shows the exclusion for higgsino-like neutralinos), and the blue area by the direct search for stau-pair production.



# References

- [1] M. Dine, W Fischler and M. Srednicki, Nucl. Phys. **B189** (1981) 575 ; S. Dimopoulos and S. Raby, Nucl. Phys. **B192** (1981) 353 ; M. Dine and W. Fischler, Phys. Lett. **B110** (1982) 227 ; M. Dine and M. Srednicki, Nucl. Phys. **B202** (1982) 238 ; L. Alvarez-Gaumé, M. Claudson and M. Wise, Nucl. Phys. **B207** (1982) 96 ; C. Nappi and B. Ovrut, Phys. Lett. **B113** (1982) 175 .
- [2] M. Dine and W. Fischler, Nucl. Phys. **B204** (1982) 346 ; S. Dimopoulos and S. Raby, Nucl. Phys. **B219** (1983) 479.
- [3] S. Dimopoulos, S. Thomas and D. Wells, hep-ph/9604452.
- [4] J. A. Bagger, K. Matchev, D. M. Pierce and R. Zhang, SLAC-PUB-7310.
- [5] D. A. Dicus, B. Dutta, S. Nandi, hep-ph/9704225 ; D. A. Dicus, B. Dutta, S. Nandi, hep-ph/9701341.
- [6] F. Borzumati, hep-ph/9702307.
- [7] Preliminary search for long lived  $\tilde{\tau}$  using the DELPHI detector, Jerusalem '97, pa 11, 13 pl 9, 15, 17.
- [8] P. Aarnio et al., Nucl. Instr. and Meth. **303** (1991) 233.
- [9] P. Abreu et al., Nucl. Instr. and Meth. **378** (1996) 57.
- [10] T. Sjöstrand, Comp. Phys. Comm. **39** (1986) 347;  
T. Sjöstrand, PYTHIA 5.6 and JETSET 7.3, CERN-TH/6488-92.
- [11] DELPHI Coll., P. Abreu *et al.*, Z. Phys. **C73** (1996) 11.
- [12] SUSYGEN 2.12, S. Katsanevas and S. Melachroinos in *Physics at LEP2*, CERN 96-01, Vol. 2, p. 328 and <http://lyohp5.in2p3.fr/delphi/katsan/susygen.html> .
- [13] DELSIM Reference Manual. DELPHI note 89-68 PROG 143, Sep. 1989 (unpublished).
- [14] J.E. Campagne and R. Zitoun, Z. Phys. **C43** (1989) 469.
- [15] S. Jadach and Z. Was, Comp. Phys. Comm. **79** (1994) 503.
- [16] F.A. Berends, R. Kleiss, W. Hollik, Nucl. Phys. **B304** (1988) 712.
- [17] F.A. Berends, R. Pittau, R. Kleiss, Comp. Phys. Comm. **85** (1995) 437.
- [18] S. Nova, A. Olshevski, and T. Todorov, *A Monte Carlo event generator for two photon physics*, DELPHI note 90-35 (1990).
- [19] F.A. Berends, P.H. Daverveldt, R. Kleiss, Comp. Phys. Comm. **40** (1986) 271, Comp. Phys. Comm. **40** (1986) 285, Comp. Phys. Comm. **40** (1986) 309.
- [20] S. Navas, P. Rebecchi and A. Trombini, DAFNE program description, DELPHI 96-46 PROG 215.

[21] S. Catani, Phys. Lett. **B269** (1991) 432 .

[22] DELPHI Note 98-7 PHYS 758.

[23] **missing reference!!**